Magnetoferroelectric phase transition induced by latent spin-lattice coupling in the geometrically frustrated magnet $CuFe_{0.95}Al_{0.05}O_2$

H. Tamatsukuri,[1,*] T. Uchihara,[2] S. Mitsuda,[2] Y. Ishii,[3] H. Nakao,[4] K. Takehana,[5] and Y. Imanaka[5]

[1] *Materials and Life Science Division, J-PARC Center, Japan Atomic Energy Agency, Tokai, Ibaraki 319-1195, Japan*
[2] *Department of Physics, Faculty of Science, Tokyo University of Science, Tokyo 162-8601, Japan*
[3] *National Institute for Materials Science, Center for Basic Research on Materials (CBRM), Synchrotron Radiation Imaging Group, 1-2-1 Sengen, Tsukuba, Ibaraki 305-0003, Japan*
[4] *Photon Factory, Institute of Materials Structure Science, High Energy Accelerator Research Organization (KEK), Tsukuba, Ibaraki 305-0801, Japan*
[5] *National Institute for Materials Science, Center for Basic Research on Materials (CBRM), High Magnetic Field Physics Group, 3-13 Sakura, Tsukuba, Ibaraki 305-0003, Japan*

(Dated: March 18, 2025)

In multiferroic $CuFe_{0.95}Al_{0.05}O_2$, applying uniaxial pressure p generates a magnetoferroelectric phase distinct from the well-studied spin-driven ferroelectric phase associated with helical magnetic ordering in this system. Using a four-circle neutron diffractometer, the magnetic structure of the p-induced magnetoferroelectric phase is determined as the collinear sinusoidal type, which itself does not break the inversion symmetry in this system. Additionally, synchrotron radiation x-ray diffraction experiments are conducted to investigate how the triangular lattice in $CuFe_{0.95}Al_{0.05}O_2$ is distorted by applied p. Although lattice distortion during the magnetic phase transition in $CuFe_{0.95}Al_{0.05}O_2$ is mitigated by the substitution of nonmagnetic Al^{3+}, the application of p along the conjugate direction revives the "latent" spin–lattice coupling, causing the triangular lattice to distort during magnetic phase transition. The application of a magnetic filed considerably reduces p-induced ferroelectric polarization, but does not affect lattice distortion. These results indicate that p-induced ferroelectric polarization is not a consequence of the piezoelectric effect. Instead, the sinusoidal magnetic structure would contribute to the emergence of p-induced ferroelectric polarization through spin-lattice coupling.

I. INTRODUCTION

In geometrically frustrated magnets, competing interactions often result in complex magnetic structures, such as spiral magnetic ordering, which break the inversion symmetry in the system[1,2]. Recent studies on magnetoelectric effects have reported that such spiral magnetic ordering can induce ferroelectric polarization driven by either spin–orbit interactions or the exchange striction effect[3–7]. Additionally, these magnetic systems tend to strongly correlate lattice degrees of freedom and spins, lifting the large ground-state degeneracy caused by frustration[8–11]. Consequently, degrees of freedom in geometrically frustrated magnet–namely charge, spin, orbital, and lattice–are potentially interconnected. The interplay between these degrees of freedom often induces exotic phenomena, such as piezomagnetoelectric effects, which can be controlled by external fields[12–19]. Delafossite $CuFeO_2$, which exhibits both spin-driven ferroelectricity and strong spin–lattice coupling, serves as an example of a system where multiple degrees of freedom are interlinked.

The crystal structure of $CuFeO_2$ belongs to the $R\bar{3}m$ space group at room temperature ($a = b = 3.03$ Å and $c = 17.17$ Å in the hexagonal notation)[20]. As shown in the inset of Fig. 1(a), Fe^{3+} in $CuFeO_2$ ($S = 5/2$) form a triangular lattice with antiferromagnetic interactions, resulting in geometrical frustration. With decreasing temperature (T), $CuFeO_2$ undergoes sequential magnetic phase transitions from the paramagnetic (PM) phase to a partially disordered (PD) phase at $T_{N1} = 14$ K and subsequently to a four-sublattice (4SL) phase at $T_{N2} = 11$ K[21,22]. Spin configurations in the PD phase and the 4SL phase are sinusoidally amplitude-modulated almost along the c axis (Fig. 1(b)) and collinear ↑↑↓↓ along the c axis (Fig. 1(c)), which are characterized by magnetic propagation wave vectors (q, q, 3/2; $q = 0.196$–0.220) (T dependent) and (1/4, 1/4, 3/2), respectively[21,22]. Substituting Fe^{3+} with a few percentage nonmagnetic Al^{3+} or Ga^{3+} induces two additional magnetic phases: the ferroelectric-incommensurate (FE-ICM) phase and the oblique-PD (OPD) phase[23–26]. A schematic of the x–T phase diagram for $CuFe_{1-x}Al_xO_2$ is illustrated in Fig. 1(a). In the FE-ICM phase, known as the spin-driven ferroelectric phase, a screw helical magnetic structure with a wave vector (q, q, 3/2; $q \sim 0.207$) breaks the spatial inversion symmetry of the system (Fig. 1(d)) and generates ferroelectric polarization P along the [110] direction[27,28]. The helicity of this magnetic structure, with its screw axis along the [110] direction, directly determines the direction of P. This relationship is well explained by the Fe $3d$–O $2p$ hybridization mechanism[29] and/or the extended inverse Dzyaloshinskii–Moriya mechanism[30,31]. Similar to that in the PD phase, the magnetic structure in the OPD phase is the sinusoidal and inclined at ∼50° from the c axis toward the [$\bar{1}$10] direction (Fig. 1(e))[32]. Unlike that in the PD phase, the value of $q = 0.195$ in the OPD phase remains independent of T[25,33].

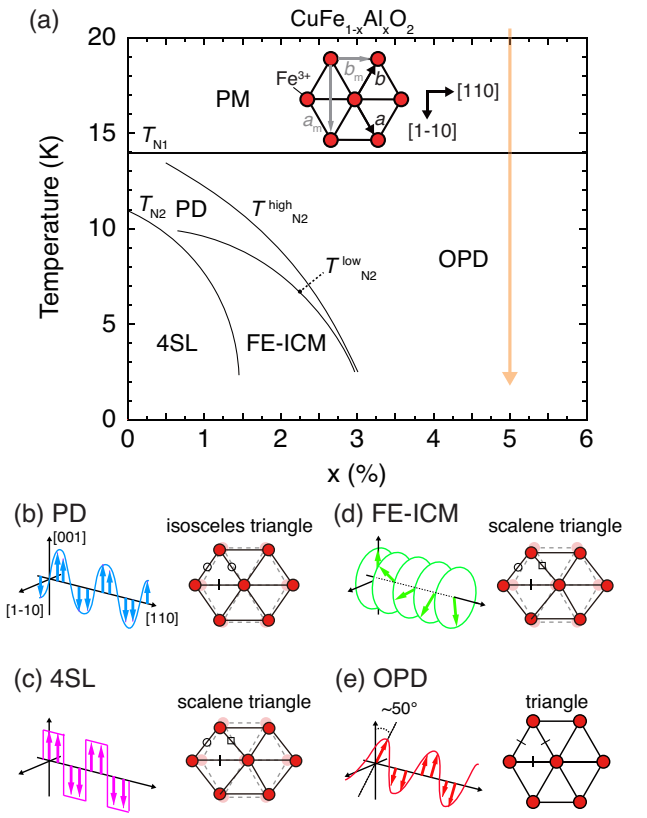

FIG. 1. Schematic x-T magnetic phase diagram of $CuFe_{1-x}Al_xO_2$. Illustrations of the magnetic structure and Fe^{3+} triangular lattice in the (b) PD, (c) 4SL, (d) FE-ICM, and (e) OPD phases.

Magnetic phase transitions in this system, except for the transition from the PM phase to the OPD phase, are accompanied by spontaneous lattice distortions that partially relieve geometrical frustration[20,34–36]. During the transition from the PM phase to the PD phase at T_{N1}, the crystal symmetry changes from hexagonal $R\bar{3}m$ to monoclinic $C2/m$[20,35] and further changes into the lower monoclinic symmetry in the 4SL and FE-ICM phase[34,37]. As shown in Figs. 1(b)–1(e), previous synchrotron radiation x–ray diffraction studies have well established triangular lattices in each of the aforementioned magnetic phases[36,38]. During lattice distortion, the hexagonal [110] (monoclinic b_m) axis elongates while the hexagonal [1$\bar{1}$0] (monoclinic a_m) axis contracts. Thus, uniaxial pressure p along the [1$\bar{1}$0] direction acts as a conjugate field to lattice distortion in this system.

Based on this relationship, the effects of p on magnetic phase transitions[39,40], lattice distortions[40,41], and spin-driven ferroelectricity[42,43] in $CuFe_{1-x}M_xO_2$ (M = Ga and Al) have been extensively investigated. In particular, applying $p \parallel [1\bar{1}0] \geq 200$ MPa, with the value of p varying with x, generates a new ferroelectric phase different from the FE-ICM phase[19,33]. Hereafter, this p-induced ferroelectric phase is referred to as the FE2 phase. Ferroelectric polarization in the FE2 phase is aligned along the [110] direction, similar to that in the FE-ICM phase, and its value is comparable with or larger than that in the FE-ICM phase[19,33]. Previous studies have reported that under applied p, PD or OPD phases become ferroelectric, with the magnetic structure of the p-induced FE2 phase apparently retaining a collinear sinusoidal configuration[19,33]. These results suggest that a collinear sinusoidal magnetic structure is essential for the emergence of the FE2 phase, irrespective of the tilt of the sinusoidal plane. However, as will be discussed in Sec. III B, using a two-axis diffractometer prevents a definitive distinction between sinusoidal and screw helical orderings. Consequently, the magnetic structure of the FE2 phase remains largely unclear. Meanwhile, the triangular lattice distorts into an isosceles shape in the PD phase even at ambient pressure, while it remains equilateral in the OPD phase, as mentioned earlier. Elucidating the deformation of the triangular lattice during transition from the OPD phase to the FE2 phase under applied p and its relationship with the ferroelectricity of the FE2 phase is critical.

In this study, to shed light on the origin of $P_{[110]}$ in the FE2 phase, we reinvestigate the magnetic structure in the FE2 phase using a four-circle neutron diffractometer, and examine how applied p distorts the triangular lattice during the transition from the OPD to the FE2 phase. $CuFe_{0.95}Al_{0.05}O_2$, indicated by an orange arrow in Fig. 1(a), is chosen as the target material because its lattice distortion during the PM-to-OPD phase transition was suppressed by the substitution of nonmagnetic Al^{3+}. The magnetic structure of the FE2 phase is identified as the collinear sinusoidal type. As such a collinear sinusoidal magnetic structure does not break the inversion symmetry, we reconfirm our previous conclusion that $P_{[110]}$ in the FE2 phase is not purely spin-driven, unlike in the FE-ICM phase. The T dependence of b_m in $CuFe_{0.95}Al_{0.05}O_2$ exhibits variations under applied p even in the PM phase and certain anomalies around T_{N1} and the OPD-to-FE2 transition temperature. These results suggest that applying p along the conjugate direction activated "latent" spin–lattice coupling, leading to triangular lattice distortion during magnetic phase transition. Such lattice distortion into at least an isosceles triangular lattice as well as the sinusoidal magnetic structure would be essential for generating the FE2 phase. These findings form the basis for discussing the origin of "spin-associated" ferroelectricity.

II. EXPERIMENTS

A single crystal of $CuFe_{0.95}Al_{0.05}O_2$ with the nominal composition was prepared using the floating zone technique[44]. The crystal was cut into a rectangular shape with typical dimensions of $1.12 \times 1.98 \times 2.60$ mm^3, in which three axes are along [110], [1$\bar{1}$0], and [001] direc-

tions.

Uniaxial pressure p was applied along the $[1\bar{1}0]$ direction using a custom-built uniaxial pressure device and pressure cell. Details regarding this equipment can be found elsewhere [39, 41, and 45]. The maximum force of our uniaxial pressure device is 2000 N. Since the pressurized area of the sample is $1.12 \times 2.60 \simeq 2.91$ mm^2, we can apply p up to 600 MPa to the sample. Except for the neutron diffraction experiment described below, p was applied at 25 K in all measurements.

The T dependence of magnetic susceptibility (χ) under a 1000 Oe magnetic field applied along the $[1\bar{1}0]$ direction was measured using a superconducting quantum interference device magnetometer (Quantum Design). The real and imaginary parts of dielectric constant, $\epsilon_{\rm r}'/\epsilon_{\rm r}''$, were obtained at 10 kHz using an LCR meter (Agilent 4980A) with silver paste electrodes applied to the [110] surfaces. Ferroelectric polarization using [110] electrodes, $P_{[110]}$, was determined by integrating the polarization current measured using an electrometer over time (Keithley 6517A). Before polarization current measurements, a poling electric field $E_{\rm p}$ (typically 240 kV/m) was applied during the cooling process, and then removed. For $P_{[110]}$ measurements under an applied magnetic filed (H) parallel to the $[1\bar{1}0]$ direction, H was generated using a 15-T superconducting magnet installed at the Tsukuba Magnet Laboratory of the National Institute for Materials Science (NIMS).

Neutron-diffraction measurements under applied p were performed using the four-circle neutron diffractometer (FONDER) installed at the JRR-3 in the Japan Atomic Energy Agency, Tokai, Japan. The incident neutron wavelength was 1.24 Å. The sample with the cramped-type pressure cell (see Sec. III B) was mounted onto a closed-cycle He-gas refrigerator, and cooled down to 3 K.

The synchrotron radiation x-ray diffraction measurements under applied p and H were performed at beamline BL-3A of the Photon Factory, High Energy Accelerator Research Organization, Tsukuba, Japan. A superconducting cryomagnet generated an H field of up to 7 T, parallel to the $[1\bar{1}0]$. The energy of the incident x-ray was set to 14 keV unless otherwise specified. Since $p \parallel [1\bar{1}0]$ was applied vertically, the scattering plane was the (H, H, L) plane.

III. RESULTS

A. Emergence of ferroelectricity under applied p in $CuFe_{0.95}Al_{0.05}O_2$

Figure 2(a) shows the T dependence of χ under applied p. $T_{\rm N1}$ increases with increasing p. This $T_{\rm N1}(p)$ agrees well with previously reported results including neutron diffraction measurements[33,40].

The application of p induces $P_{[110]}$, accompanied by a significant increase in $\epsilon_{\rm r}'/\epsilon_{\rm r}''$ and large thermal hysteresis

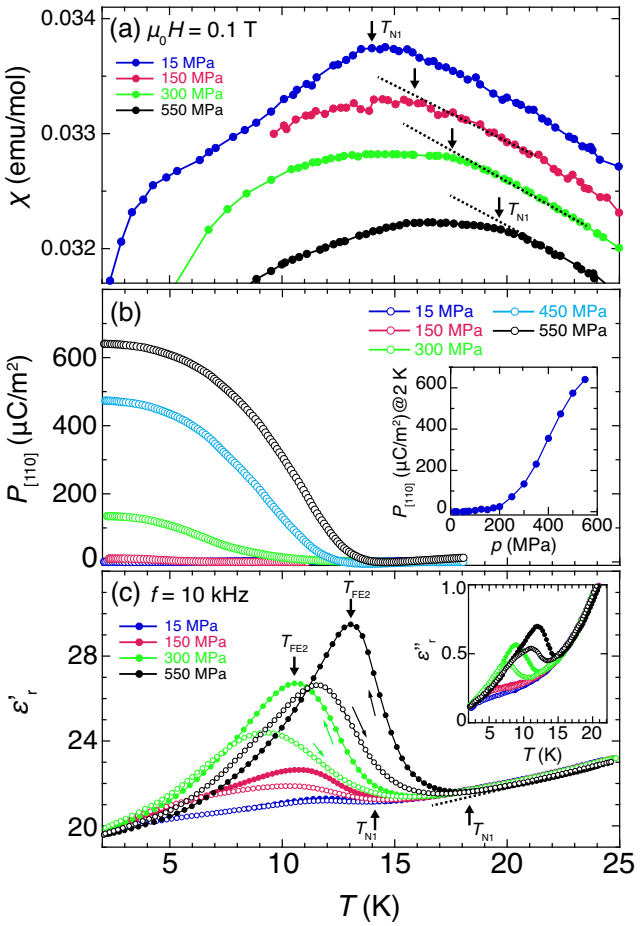

FIG. 2. Temperature dependence of (a) χ, (b) $P_{[110]}$, and (c) $\epsilon_{\rm r}'$ under specific applied p. The insets in (b) and (c) depict the value of the $P_{[110]}$ at 2 K as a function of p and the T dependence of $\epsilon_{\rm r}''$, respectively. For clarity, the χ data for p = 150, 300, and 550 MPa are vertically offset .

at the emergence temperature, as shown in Figs. 2(b) and 2(c). Around $T_{\rm FE2}$ where $P_{[110]}$ appears or disappears, $\epsilon_{\rm r}'$ exhibits a peak. Notably, the $\epsilon_{\rm r}'$ peak temperature during cooling is apparently closer to $T_{\rm FE2}$ than that during heating, although $P_{[110]}$ are measured on the heating run. The ferroelectricity of $P_{[110]}$ is evidenced by the polarity reversal with dependence on the sign of $E_{\rm p}$ (see Fig. 4(b)). We add that $T_{\rm N1}$ can be determined also by deviation from the linear T dependence of $\epsilon'(T)$ in the PM phase. The above results are summarized in the p–T phase diagram in Fig. 3, which align well with previously reported results[33]. The slight differences, such as the smaller $T_{\rm FE2}$ and the smaller threshold pressure of the emergence of the FE2 phase, would be due to the slight difference in the Al concentration. The threshold region of the emergence of the FE2 phase are described in the Sec. VI A.

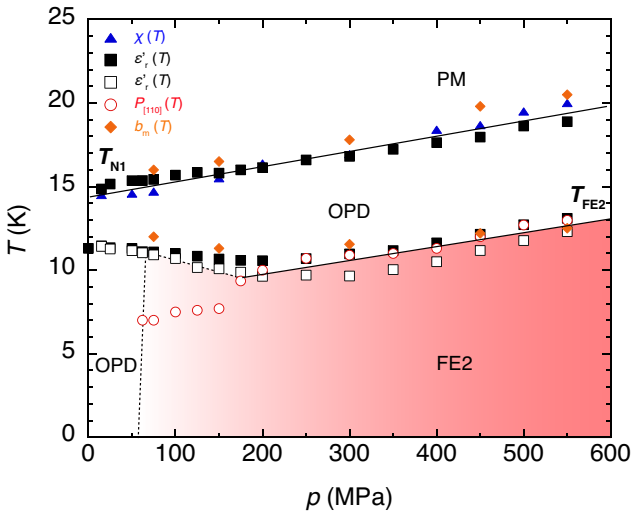

FIG. 3. Temperature (T) vs. uniaxial pressure ($p \parallel [1\bar{1}0]$) magnetic–electric phase diagram of $CuFe_{0.95}Al_{0.05}O_2$. Open and closed symbols represent data obtained under conditions of increasing and decreasing T, respectively.

B. Magnetic structure in the FE2 phase

Next, we investigate the magnetic structure of the FE2 phase, which is crucial for determining whether $P_{[110]}$ in this phase results from spin-driven ferroelectricity. Preliminary magnetic structure analysis conducted in our previous study revealed that the magnetic structure of the FE2 phase was not of the cycloidal type, which is widely observed in spin-driven ferroelectrics, but resembled or was nearly identical to the PD or OPD magnetic structures[33]. However, this study was restricted to magnetic reflections in the (H, H, L) zone of the reciprocal lattice space[33]. Within the (H, H, L) zone, *"the spin orientation factor"* (SOF) described below is symmetric with respect to L for both the FE-ICM and the PD(OPD) models[27,32]. Consequently, it remains unclear whether the magnetic structure of the FE2 phase definitively differs from the screw helical structure seen in the FE-ICM phase[27,32]. To address this limitation, we employ a four-circle neutron diffractometer and a cramped-type uniaxial pressure cell, as shown in Fig. 4(a). This pressure cell is required to pressurize the sample at room temperature, and the effective pressure applied to the sample becomes uncertain after cooling. Hence, before the neutron diffraction measurements, we confirm the emergence of $P_{[110]}$ (Fig. 4(b)) and estimate the effective magnitude of applied p based on the results of $P_{[110]}$ and ϵ'_r measurements. Judging from T_{FE2}, the value of $P_{[110]}$, and enhancement in ϵ'_r (Fig. 4(c)), the magnitude of applied p is estimated to be ∼200 MPa. Note that the absolute value of ϵ'_r differs from the data presented in Fig. 2(c). This difference likely originate from variations in electrode conditions. However, the relative enhancements in ϵ'_r are consistent across measurements.

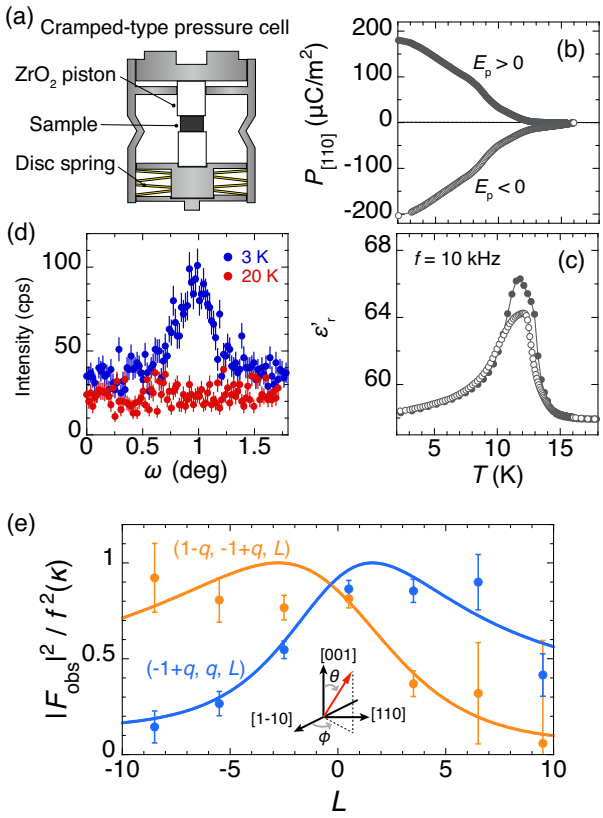

FIG. 4. (a) Schematic drawing of the cramped-type uniaxial pressure cell. Using CuBe disk springs, p was applied at room temperature and maintained throughout the entire experiments. T dependence of (b) $P_{[110]}$ and (c) ϵ'_r under applied p determined using the cramped-type uniaxial pressure cell. (d) Typical neutron diffraction profiles recorded at (−0.804, 0.196, 0.5) under applied p at 3 K and 20 K. (e) Index L dependence of $|F_{obs}|^2/f^2(\kappa)$ for the $(1-q, -1+q, L)$ and $(-1+q, q, L)$ magnetic Bragg points, where $q = 0.196$. Solid curves represent the fitting results for the oblique sinusoidal model (OPD model). The inset shows a schematic of the magnetic moment direction (red arrow) in the OPD model.

Figure 4(d) shows the typical neutron diffraction profiles at $(-1+q, q, 0.5; q = 0.196)$ under applied p at 3 K and 20 K. Fourteen magnetic reflections outside the (H, H, L) plane were successfully observed. The magnetic structure factor $|F|^2_{HKL}$ is described as

$$|F|^2_{HKL} = \gamma_0^2 f(\kappa)^2 \mu^2 \cdot \mathrm{SOF}, \quad (1)$$

where $\gamma_0 = -0.54 \times 10^{-12}$ cm and μ, κ, and $f(\kappa)$ denote the amplitude of the magnetic moment, a magnitude of the scattering vector, and a magnetic form factor of Fe^{3+}, respectively[27,32,46]. Thus, $|F|^2_{obs}/f(\kappa)^2$ is proportional to the SOF. Here, $|F|_{obs}$ represents the observed magnetic structure factor. Following Refs. [27] and [32], we compare $|F|^2_{obs}/f(\kappa)^2$ with the calculated SOF.

Figure 4(e) shows the estimated L dependence of $|F|^2_{obs}/f(\kappa)^2$, which is clearly asymmetric. For proper

TABLE I. Estimated angle parameters for the oblique sinusoidal model.

	T (K)	θ (deg.)	ϕ (deg.)	μ (μ_B)
FE2	4.5	28 ± 5	-4 ± 5	4 (fixed)
OPD [32]	9	51 ± 11	-2 ± 14	1.52 ± 0.13

screw helical ordering in the FE-ICM phase, these curves remain symmetric with respect to L even outside the (H, H, L) plane[27,32]. This asymmetry explicitly indicates that the magnetic structure and the associated mechanism of spin-related ferroelectricity in the FE2 phase differ from those in the FE-ICM phase. Because the FE2 phase was previously suggested to have a sinusoidal magnetic structure, we employ an oblique sinusoidal model as our least-squares fitting function. Owing to the limited number and low intensity of magnetic reflections arising from the small sample size, we fixed the moment size at 4 μ_B[27] and estimate the angle parameters in the oblique sinusoidal model. These parameters are summarized in Table I. For a constant moment size, the fit is acceptable within an accuracy and uncertainty range comparable to that in prior analyses. Considering the large error margins, there exists almost no difference in ϕ between the two phases. In contrast, θ is markedly reduced in the FE2 phase, indicating that the original OPD magnetic structure moves closer to the PD magnetic structure.

This inclined sinusoidal magnetic structure does not break inversion symmetry in this system, because of the remaining mirror plane perpendicular to the [110] axis. Here, we emphasize that the values of the p-induced $P_{[110]}$ are comparable to those in other spin-driven ferroelectric materials[3–7]. Given the significant uncertainty of the magnetic structure analysis in this study, minor modifications from the PD(OPD) ordering could, in principle, break inversion symmetry. However, it seems unlikely that such minute alterations would yield a $P_{[110]}$ comparable to those in other spin-driven ferroelectric materials. We therefore reaffirm our previous conclusion that $P_{[110]}$ in the FE2 phase is not purely spin–driven as in the FE-ICM phase.

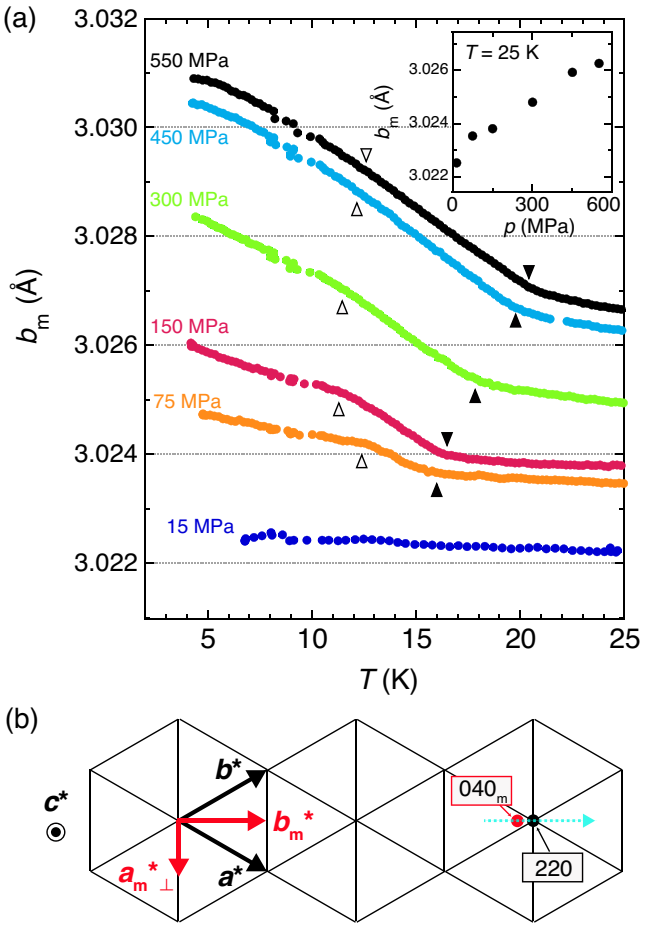

FIG. 5. (a) T dependence of b_m under applied p. Error bars are within the size of the symbols. All data were recorded under conditions of decreasing T. The inset presents the b_m values at 25 K as a function of p. Anomalies around T_{FE2} (indicated by open triangles) were identified by deviations from the linear $b_m(T)$ dependence in the OPD phase (see the inset of Fig.6), although these anomalies are difficult to discern at the vertical scale used in this figure. (b) Reciprocal lattice map of $CuFe_{0.95}Al_{0.05}O_2$ showing the relationship between the 040_m and 220 Bragg reflections. In the absence of the lattice distortion, the 040_m and 220 reciprocal lattice points coincide. The horizontal dashed arrow denotes the scan direction. $a^*_{m\perp}$ denotes the c-plane projection of a^*_m, which corresponds to the pressure direction.

C. Lattice distortion induced by applied p in $CuFe_{0.95}Al_{0.05}O_2$

Figure 5(a) shows the T dependence of b_m under applied p, which is estimated from the 040_m Bragg reflection using the method used in a previous study[40,41]. Since we define $a_m = a - b$ and $b_m = a + b$ (see the inset of Fig. 1(a)), b^*_m lies on the a^*–b^* plane; namely, the elongation of the hexagonal [110] axis by applied $p \parallel [1\bar{1}0]$ corresponds to the change in b_m (b^*_m), as shown in Fig. 5(b). At near-zero pressure (15 MPa), no anomalies in $b_m(T)$ are apparent at $T_{N1} = 14$ K, indicating that the triangular lattice does not distort during the transition into the OPD phase[36]. As shown in the inset of Fig. 5, the value of b_m at 25 K increases linearly with p, consistent with observations in other $CuFe_{1-x}M_xO_2$ compositions[40,41]. This result implies that the triangular lattice of $CuFe_{0.95}Al_{0.05}O_2$ is distorted by p even in the PM phase. Note that the magnitude of this distortion induced by applied p at 25 K is comparable to that of the spontaneous lattice distortion occurring during the PM-to-4SL phase transition in $CuFeO_2$ at ambient pressure[34,40]. Because the 030_m superlattice reflection, an indicator of scalene triangular distortion[37,40], is not

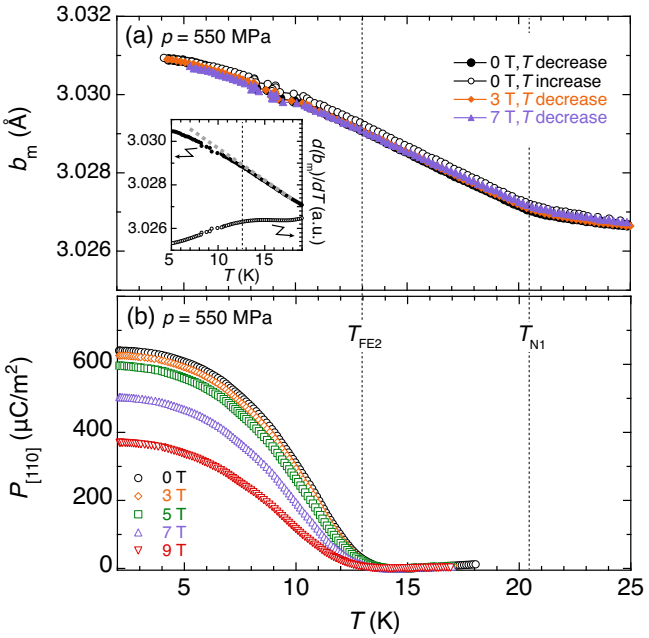

FIG. 6. Magnetic-field-induced variations in (a) $b_{\rm m}$ and (b) $P_{[110]}$ under applied $p = 550$ MPa as a function of T. Open and closed symbols represent data measured with increasing and decreasing T, respectively. The magnetic filed is applied parallel to the $[1\bar{1}0]$ direction ($\parallel p$). The inset in (a) shows a magnified view of $b_{\rm m}(T)$ (0 T, T decrease) and its T–derivative.

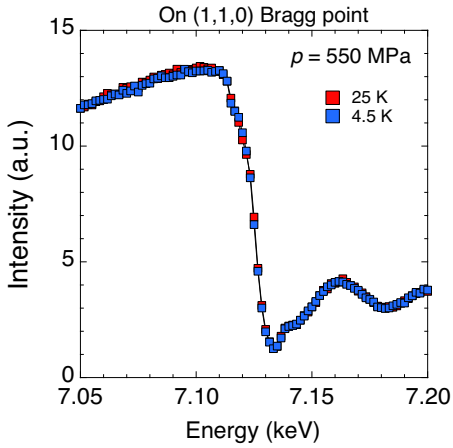

FIG. 7. Energy dependence of scattering intensities at the $(1, 1, 0)$ Bragg point near the Fe K edge. Data are recoded at 25 K and 4.5 K under applied $p = 550$ MPa and normalized by the value at 7.05 keV. Error bars are within the size of symbols.

observed down to the lowest temperature, the triangular lattice in the FE2 phase is inferred to remain isosceles.

With decreasing T, $b_{\rm m}(T)$ under applied p, particularly below 300 MPa, exhibits anomalies near both $T_{\rm N1}$ and $T_{\rm FE2}$. These temperatures are plotted in the p–T phase diagram shown in Fig. 3. The upward kinks at $T_{\rm N1}$ resemble those observed in other $CuFe_{1-x}M_xO_2$ compositions[40,41]. Although spin–lattice coupling is suppressed by the substitution of nonmagnetic Al^{3+}, the application of p along the conjugate direction appears to activate "latent" spin–lattice coupling, causing the triangular lattice to distort during magnetic phase transition in $CuFe_{0.95}Al_{0.05}O_2$. Additionally, the anomaly in $b_{\rm m}(T)$ near $T_{\rm FE2}$ corresponds to the peak structure in $\epsilon'(T)$, even within the ambiguous emergence region around p = 75 MPa. These results suggest that lattice distortion into at least an isosceles triangular lattice is essential for the emergence of the FE2 phase, alongside the sinusoidal magnetic structure. As can be seen in the inset of Fig. 6, the anomalies in $b_{\rm m}(T)$ at $T_{\rm FE2}$ in $b_{\rm m}(T)$ under p of 450 and 550 MPa are detectable but rather small. This observation further supports the conclusion that p acts as a "conjugate" field to lattice distortion in this system, similar to the T dependence of magnetization under an applied magnetic field.

Figure 6 shows the T dependence of $b_{\rm m}$ and $P_{[110]}$ under applied $p = 550$ MPa and a magnetic field. In addition to the absence of thermal hysteresis, $b_{\rm m}(T)$ under this applied pressure remains unaffected by the magnetic field. Conversely, the magnetic field significantly reduces the magnitude of $P_{[110]}$ in the FE2 phase. These results indicate that $P_{[110]}$ in the FE2 phase is not caused by the piezoelectric effect. Instead, the sinusoidal magnetic structure likely contributes to the emergence of $P_{[110]}$ in the FE2 phase through spin–lattice coupling.

IV. DISCUSSION

Having established that p-induced $P_{[110]}$ in the FE2 phase is neither a consequence of purely spin-driven ferroelectricity nor the piezoelectric effect, we now discuss its origin. Given that our magnetic structure analyses have revealed that the magnetic structure of the FE2 phase is neither cycloidal nor helical, mechanisms requiring spiral magnetic ordering, such as the spin current model and the extended inverse Dzyaloshinskii–Moriya model, would be excluded as potential explanations for the origin of $P_{[110]}$ in the FE2 phase. Thus, the most plausible mechanism would be the exchange striction model, which involves the induction of ferroelectric polarization in collinear magnetic structures[7]. However, in $CuFeO_2$, analyses of the magnetoelectric coupling coefficients in the generalized bilinear function of spin components have revealed that collinear magnetic structures (4SL and PD phases) do not induce $P_{[110]}$[31]. Furthermore, this model originally requires the spin modulation to be commensurate with the lattice structure[7,29]. Therefore, in the context of the exchange striction model, it is somewhat puzzling that the PD and OPD phases become ferroelectric under applied p whereas the 4SL phase does not[19,33,40].

To investigate whether the application of p affects

charge transfer from Fe^{3+} to O^{2-} depending on the magnetic structure, we tentatively examine the energy dependence of x-ray scattering intensities. Resonant x-ray scattering (RXS) spectra are proportional to the square of the atomic scattering factor, given by $f_0(\boldsymbol{Q})+f'(E)+if''(E)$, where $f_0(\boldsymbol{Q})$, $f'(E)$, and $f''(E)$ denote the Thomson scattering factor, real part of the anomalous scattering factor, and imaginary part of the anomalous scattering factor, respectively. The anomalous scattering factor changes significantly near the absorption edge energy, reflecting electronic state changes during the absorption process. Also, the absorption edge energy is sensitive to the valence state of ions. Figure 7 illustrates the RXS spectra at the $(1, 1, 0)$ Bragg point near the Fe K edge under applied $p = 550$ MPa. Although these data correspond to the Fe K edge ($1s \rightarrow 4p$), significant changes in the $3d$ states would be expected to slightly affect the $4p$ states. However, the RXS spectra of the PM (25 K) and FE2 (4.5 K) phases show almost no changes near the absorption edge energy. Moreover, no signals are observed in the so-called pre-edge region ($1s \rightarrow 3d$) on the lower energy side. These results suggest that the application of p does not significantly modify the electronic configuration of the FE2 phase.

Even in pure $CuFeO_2$, the PD phase becomes the FE2 phase upon the application of p[19]. However, in this system, the induction of $P_{[110]}$ requires the combined application of p and a magnetic field H[19]. Based on this observation, we have proposed that the induction of $P_{[110]}$ through the combined application of p and H can be regarded as a nonlinear piezomagnetoelectric effect[19]. In this study, we have argued that the application of H introduces a site-dependent modulation of the magnetic moment magnitudes, specifically in the PD phase, which may be a critical factor for the nonlinear piezomagnetoelectric effect. Additionally, we have noted that because nonmagnetic impurities influence geometrically frustrated magnets by acting as an effective random field[47–49], substituting Fe^{3+} with Al^{3+} introduces site-random effects that function analogously to a magnetic field to some extent. This creates conditions similar to the site-dependent modulation of magnetic moments by H[19]. Therefore, the results of Al-doped $CuFeO_2$ without H may be understood as a similar effect of the nonlinear piezomagnetoelectric effect.

However, the response of p-induced $P_{[110]}$ to H differs between $CuFe_{0.95}Al_{0.05}O_2$ and $CuFeO_2$. Specifically, H significantly reduces the magnitude of $P_{[110]}$ in $CuFe_{0.95}Al_{0.05}O_2$ as described above, while in $CuFeO_2$, H is essential for the emergence of the FE2 phase and facilitates the induction of $P_{[110]}$[19]. To fully understand this phenomenon, further investigations, including theoretical calculations, are necessary.

V. SUMMARY AND CONCLUSION

We reinvestigate the magnetic structure in the FE2 phase in $CuFe_{0.95}Al_{0.05}O_2$ using the four-circle neutron diffractometer, and examine how the triangular lattice in this system is distorted by applied p as the OPD phase transitions into the FE2 phase. The magnetic structure of the FE2 phase is determined to be the collinear sinusoidal type. The application of p along the conjugate direction activates the "latent" spin–lattice coupling in $CuFe_{0.95}Al_{0.05}O_2$, causing the triangular lattice to distort during magnetic phase transition. This suggests that lattice distortion into at least an isosceles triangular lattice, alongside the sinusoidal magnetic structure, is essential for the emergence of the FE2 phase. The T dependence of $b_{\rm m}$ and $P_{[110]}$ under applied p and a magnetic filed indicates that the p-induced ferroelectric polarization is not a consequence of the piezoelectric effect. Instead, the sinusoidal magnetic structure would contribute to the emergence of p-induced ferroelectric polarization through spin–lattice coupling. To elucidate the origin of this "spin-associated" ferroelectricity, further investigations, including theoretical calculations, are necessary.

ACKNOWLEDGMENTS

H.T., T.U., and S.M. thank late Hiroyuki Kimura for his support during the neutron diffraction experiments performed at JRR-3. The neutron diffraction experiments at JRR-3 and x-ray scattering experiments performed at the Photon Factory were conducted under Proposal Nos. NSL00001213 and 2021G093, respectively. This work was supported by JSPS KAKENHI (Grant No. JP20K14421) and the NIMS Joint Research Hub Program.

VI. APPENDIX

A. Threshold pressure for the emergence of the FE2 phase

Figure 8(a) shows the T dependence of $P_{[110]}$ under applied p near the emergence zone of the FE2 phase. The sample used for the present $P_{[110]}$ measurements exhibits relatively low resistivity, causing leakage currents that complicates the subtraction of the background signal. Combined with the small $P_{[110]}$ values at the emergence point of the FE2 phase, this contributes to deviations in the $T_{\rm FE2}$ values determined from $P_{[110]}(T)$ relative to those derived from other physical quantities.

Figure 8(b) shows the p dependence of $P_{[110]}$ at 2 K on a logarithmic scale. $P_{[110]}(T)$ appears to be gradually induced under the application of p, rather than resulting from an abrupt phase transition. As shown in Fig. 2(c), $\epsilon'(T)$ displays a small hump in the temperature region

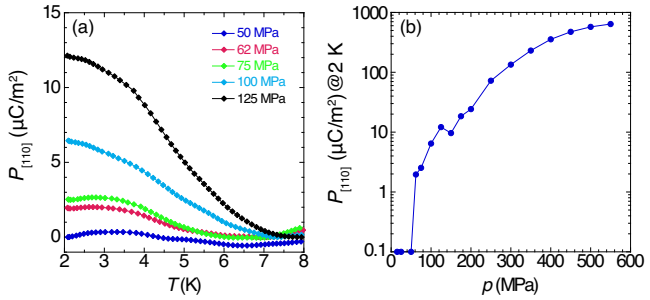

FIG. 8. (a) T dependence of $P_{[110]}$ under applied p near the emergence region of the FE2 phase. (b) p dependence of $P_{[110]}$ at 2 K on a logarithmic scale, showing the same data as in the inset in Fig. 2(b).

of the OPD phase even at ambient pressure, which becomes more pronounced as a signature of the transition into the FE2 phase when p exceeds 200 MPa. The magnetic and electric states of the OPD phase may be on the verge of transitioning into the FE2 phase even at ambient pressure.

* E-mail address: hiromu.tamatsukuri@j-parc.jp

[1] J. E. Greedan, Geometrically frustrated magnetic materials, J. Mater. Chem. **11** (2001).

[2] R. Moessner and A. P. Ramirez, Geometrical frustration, Phys. Today **59**, 24 (2006).

[3] T. Kimura, T. Goto, H. Shintani, K. Ishizaka, T. Arima, and Y. Tokura, Magnetic control of ferroelectric polarization, Nature (London) **426**, 55 (2003).

[4] W. Eerenstein, N. D. Mathur, and J. F. Scott, Multiferroic and magnetoelectric materials, Nature (London) **442**, 759 (2006).

[5] T. Kimura and Y. Tokura, Magnetoelectric phase control in a magnetic system showing cycloidal/conical spin order, J. Phys.: Condens. Matter **20**, 434204 (2008).

[6] T. Arima, Spin-Driven Ferroelectricity and Magneto-Electric Effects in Frustrated Magnetic Systems, J. Phys. Soc. Jpn. **80**, 052001 (2011).

[7] Y. Tokura, S. Seki, and N. Nagaosa, Multiferroics of spin origin, Rep. Prog. Phys. **77**, 076501 (2014).

[8] Y. Yamashita and K. Ueda, Spin-Driven Jahn-Teller Distortion in a Pyrochlore System, Phys. Rev. Lett. **85**, 4960 (2000).

[9] F. Becca and F. Mila, Peierls-Like Transition Induced by Frustration in a Two-Dimensional Antiferromagnet, Phys. Rev. Lett. **89**, 037204 (2002).

[10] D. L. Bergman, R. Shindou, G. A. Fiete, and L. Balents, Models of degeneracy breaking in pyrochlore antiferromagnets, Phys. Rev. B **74**, 134409 (2006).

[11] F. Wang and A. Vishwanath, Spin Phonon Induced Collinear Order and Magnetization Plateaus in Triangular and Kagome Antiferromagnets: Applications to $CuFeO_2$, Phys. Rev. Lett. **100**, 077201 (2008).

[12] H. Grimmer, The Piezomagnetoelectric Effect, Acta. Cryst. **A48**, 266 (1992).

[13] J. P. Rivera and H. Schmid, Search for the piezomagnetoelectric effect in $LiCoPO_4$, Ferroelectrics **161**, 91 (1994).

[14] T. Naka jima, Y. Tokunaga, V. Ko csis, Y. Taguchi, Y. Tokura, and T. Arima, Uniaxial-Stress Control of Spin-Driven Ferroelectricity in Multiferroic $Ba_2CoGe_2O_7$, Phys. Rev. Lett. **114**, 067201 (2015).

[15] T. Nakajima, Y. Tokunaga, Y. Taguchi, Y. Tokura, and T. Arima, Piezomagnetoelectric Effect of Spin Origin in Dysprosium Orthoferrite, Phys. Rev. Lett. **115**, 197205 (2015).

[16] V. D. Fil, M. P. Kolodyazhnaya, G. A. Zvyagina, I. V. Bilych, and K. R. Zhekov, Piezomagnetoelectric effect in $LiCoPO_4$, Phys. Rev. B **96**, 180407 (2017).

[17] Y. Shiomi, H. Watanabe, H. Masuda, H. Takahashi, Y. Yanase, and S. Ishiwata, Observation of a Magnetopiezoelectric Effect in the Antiferromagnetic Metal $EuMnBi_2$, Phys. Rev. Lett. **122**, 127207 (2019).

[18] T. N. Gaydamak, I. A. Gudim, G. A. Zvyagina, I. V. Bilych, N. G. Burma, K. R. Zhekov, and V. D. Fil, Magnetopiezoelectric effect and magnetocapacitance in $SmFe_3(BO_3)_4$, Phys. Rev. B **92**, 214428 (2015).

[19] H. Tamatsukuri, S. Mitsuda, T. Shimizu, M. Fujihala, H. Yokota, K. Takehana, Y. Imanaka, A. Nakao, and K. Munakata, Nonlinear piezomagnetoelectric effect in $CuFeO_2$, Phys. Rev. B **100**, 201105 (2019).

[20] F. Ye, Y. Ren, Q. Huang, J. A. Fernandez-Baca, P. Dai, J. W. Lynn, and T. Kimura, Spontaneous spin-lattice coupling in the geometrically frustrated triangular lattice antiferromagnet $CuFeO_2$, Phys. Rev. B **73**, 220404(R) (2006).

[21] M. Mekata, N. Yaguchi, T. Takagi, T. Sugino, S. Mitsuda, H. Yoshizawa, N. Hosoito, and T. Shinjo, Successive Magnetic Ordering in $CuFeO_2$ –A New Type of Partially Disordered Phase in a Triangular Lattice Antiferromagnet–, J. Phys. Soc. Jpn. **62**, 4474 (1993).

[22] S. Mitsuda, N. Kasahara, T. Uno, and M. Mase, Partially Disordered Phase in Frustrated Triangular Lattice Antiferromagnet $CuFeO_2$, J. Phys. Soc. Jpn. **67**, 4026 (1998).

[23] S. Seki, Y. Yamasaki, Y. Shiomi, S. Iguchi, Y. Onose, and Y. Tokura, Impurity-doping-induced ferroelectricity in the frustrated antiferromagnet $CuFeO_2$, Phys. Rev. B **75**, 100403(R) (2007).

[24] N. Terada, S. Mitsuda, T. Fujii, K. Soejima, I. Doi, H. A. Katori, and Y. Noda, Magnetic Phase Diagram of the Triangular Lattice Antiferromagnet $CuFe_{1-x}Al_xO_2$, J. Phys. Soc. Jpn. **74**, 2604 (2005).

[25] N. Terada, T. Naka jima, S. Mitsuda, H. Kitazawa, K. Kaneko, and N. Metoki, Ga-substitution-induced single ferroelectric phase in multiferroic $CuFeO_2$, Phys. Rev. B **78**, 014101 (2008).

[26] N. Terada, T. Nakajima, S. Mitsuda, and H. Ki-

tazawa, Magnetic phase diagram of multiferroic delafossite $CuFe_{1-y}Ga_yO_2$, J. Phys. Conf. Ser. **145**, 012071 (2009).

[27] T. Naka jima, S. Mitsuda, S. Kanetsuki, K. Prokes, A. Podlesnyak, H. Kimura, and Y. Noda, Spin Noncollinearlity in Multiferroic Phase of Triangular Lattice Antiferromagnet $CuFe_{1-x}Al_xO_2$, J. Phys. Soc. Jpn. **76**, 043709 (2007).

[28] T. Nakajima, S. Mitsuda, S. Kanetsuki, K. Tanaka, K. Fujii, N. Terada, M. Soda, M. Matsuura, and K. Hirota, Electric polarization induced by a proper helical magnetic ordering in a delafossite multiferroic $CuFe_{1-x}Al_xO_2$, Phys. Rev. B **77**, 052401 (2008).

[29] T. Arima, Ferroelectricity Induced by Proper-Screw Type Magnetic Order, J. Phys. Soc. Jpn. **76**, 073702 (2007).

[30] T. A. Kaplan and S. D. Mahanti, Canted-spin-caused electric dipoles: A local symmetry theory, Phys. Rev. B **83**, 174432 (2011).

[31] J. T. Zhang, C. Ji, J. L. Wang, W. S. Xia, B. X. Guo, X. M. Lu, and J. S. Zhu, Spin-induced ferroelectricity in a triangular-lattice antiferromagnet studied by magnetoelectric coupling tensors, Phys. Rev. B **96**, 235136 (2017).

[32] N. Terada, T. Kawasaki, S. Mitsuda, H. Kimura, and Y. Noda, Reinvestigation of Magnetic Structures for the Thermally Induced States of $CuFe_{1-x}Al_xO_2$ ($x = 0.00$, 0.02 and 0.05) Using a Four-Circle Neutron Diffractometer, J. Phys. Soc. Jpn. **74**, 1561 (2005).

[33] H. Tamatsukuri, S. Mitsuda, T. Nakamura, K. Takata, T. Nakajima, K. Prokes, F. Yokaichiya, and K. Kiefer, Spin-lattice-coupling-mediated magnetoferroelectric phase transition induced by uniaxial pressure in multiferroic $CuFe_{1-x}M_xO_2$ (M = Ga, Al), Phys. Rev. B **95**, 174108 (2017).

[34] N. Terada, S. Mitsuda, H. Ohsumi, and K. Tajima, "Spin-Driven" Crystal Lattice Distortion in Frustrated Magnet $CuFeO_2$: Synchrotron X-ray Diffraction Study, J. Phys. Soc. Jpn. **75**, 023602 (2006).

[35] G. Quirion, M. J. Tagore, M. L. Plumer, and O. A. Petrenko, Evidence of soft modes in magnetoelectric $CuFeO_2$: Ultrasonic velocity measurements and Landau theory, Phys. Rev. B **77**, 094111 (2008).

[36] T. Nakajima, S. Mitsuda, T. Inami, N. Terada, H. Ohsumi, K. Prokes, and A. Podlesnyak, Identification of microscopic spin-polarization coupling in the ferroelectric phase of magnetoelectric multiferroic $CuFe_{1-x}Al_xO_2$, Phys. Rev. B **78**, 024106 (2008).

[37] N. Terada, S. Mitsuda, Y. Tanaka, Y. Tabata, K. Katsumata, and A. Kikkawa, Field-induced Incommensurate Lattice Modulations in the Delafossite $CuFeO_2$, J. Phys. Soc. Jpn. **77**, 054701 (2008).

[38] N. Terada, Y. Tanaka, Y. Tabata, K. Katsumata, A. Kikkawa, and S. Mitsuda, Restoring Higher Symmetric Crystal Structure with Magnetic Field in Triangular Lattice Antiferromagnet $CuFeO_2$, J. Phys. Soc. Jpn. **75**, 113702 (2006).

[39] T. Nakajima, S. Mitsuda, K. Takahashi, K. Yoshitomi, K. Masuda, C. Kaneko, Y. Honma, S. Kobayashi, H. Kitazawa, M. Kosaka, N. Aso, Y. Uwatoko, N. Terada, S. Wakimoto, M. Takeda, and K. Kakurai, Uniaxial-Pressure Control of Magnetic Phase Transitions in a Frustrated Magnet $CuFe_{1-x}Ga_xO_2$ ($x = 0, 0.018$), J. Phys. Soc. Jpn. **81**, 094710 (2012).

[40] H. Tamatsukuri, S. Aoki, S. Mitsuda, T. Nakajima, T. Nakamura, T. Itabashi, S. Hosaka, S. Ito, Y. Yamasaki, H. Nakao, K. Prokes, and K. Kiefer, Uniaxial pressure effects on spin-lattice coupled phase transitions in a geometrical frustrated magnet $CuFeO_2$, Phys. Rev. B **94**, 174402 (2016).

[41] T. Nakajima, Y. Iguchi, H. Tamatsukuri, S. Mitsuda, Y. Yamasaki, H. Nakao, and N. Terada, Uniaxial-Pressure Effects on Spin-Driven Lattice Distortions in Geometrically Frustrated Magnets $CuFe_{1-x}Ga_xO_2$ ($x = 0, 0.035$), J. Phys. Soc. Jpn. **82**, 114711 (2013).

[42] S. Mitsuda, K. Yoshitomi, T. Nakajima, C. Kaneko, H. Yamazaki, M. Kosaka, N. Aso, Y. Uwatoko, Y. Noda, M. Matsuura, N. Terada, S. Wakimoto, M. Takeda, and K. Kakurai, Uniaxial-stress enhancement of spin-driven ferroelectric polarization in a multiferroic $CuFe_{1-x}Ga_xO_2$, J. Phys.: Conf. Ser. **340**, 012062 (2012).

[43] T. Nakajima, S. Mitsuda, T. Nakamura, H. Ishii, T. Haku, Y. Honma, M. Kosaka, N. Aso, and Y. Uwatoko, Control of ferroelectric polarization via uniaxial pressure in the spin-lattice-coupled multiferroic $CuFe_{1-x}Ga_xO_2$, Phys. Rev. B **83**, 220101 (2011).

[44] T. R. Zhao, M. Hasegawa, and H. Takei, Crystal growth and characterization of cuprous ferrite ($CuFeO_2$), J. Cryst. Growth **166**, 408 (1996).

[45] T. Kozawa, M. Fujihala, T. Uchihara, S. Mitsuda, S. Yano, H. Tamatsukuri, K. Munakata, and A. Nakao, Atomic reconstruction induced by uniaxial stress in MnP, Scientific Reports **13**, 13750 (2023).

[46] G. L. Squires, *Introduction to the theory of Thermal Neutron Scattering* (Cambridge University Press, New York) (2012).

[47] J. van Duijn, B. D. Gaulin, M. A. Lumsden, J. P. Castellan, and W. J. L. Buyers, Random Fields and the Partially Paramagnetic State of $CsCo_{0.83}Mg_{0.17}Br_3$: Critical Scattering Study, Phys. Rev. Lett. **92**, 077202 (2004).

[48] M. Mekata, T. Tatsumi, T. Nakashima, K. Adachi, and Y. Ajiro, Non-Magnetic Impurity Effect on the Spin Frustration in $CsCoCl_3$, J. Phys. Soc. Jpn. **56**, 4544 (1987).

[49] T. Nakajima, S. Mitsuda, K. Kitagawa, N. Terada, T. Komiya, and Y. Noda, Zero-field random-field effect in diluted triangular lattice antiferromagnet $CuFe_{1-x}Al_xO_2$, J. Phys.: Condens. Matter **19**,145216 (2007).